UNDERSTANDING AND DEVELOPMENT OF A PREDICTION METHOD OF TRANSONIC LIMIT CYCLE OSCILLATION CHARACTERISTICS OF FIGHTER AIRCRAFT

Jos J. Meijer
National Aerospace Laboratory (NLR), The Netherlands
Atlee M. Cunningham, Jr.
General Dynamics, Fort Worth, Texas

Abstract

An analysis of steady wind tunnel data, obtained for a fighter type aircraft, has indicated that shock-induced and trailing-edge separation play a dominant role in the development of Limit Cycle Oscillations (LCO) at transonic speeds. On the basis of these data a semi-empirical LCO prediction method is being developed. Its preliminary version has been applied to several configurations and has correctly identified those which have encountered LCO. It has already shown the potential for application early in the design process of new aircraft to determine and understand the nonlinear aeroelastic characteristics. The method has been upgraded since. It will be described in its present form and results of the latest predictions will be used to further assess various parametric effects. The ultimate refinements are expected from recent unsteady wind tunnel force and pressure measurements for which a few preliminary analyses are presented.

I. Introduction

Requirements of fighter aircraft to operate with high maneuverability in the transonic speed regime increase the potential to encounter a transonic nonlinear flutter, known as limit cycle oscillations (LCO). LCO is a limited amplitude self-sustaining oscillation produced by a structural/aerodynamic interaction. The phenomenon is related to buffet but has characteristics similar to classical flutter in that it usually occurs at a single frequency. From an operational point of view, LCO results in an undesirable airframe vibration that limits the pilot's functional abilities and produces extreme discomfort and anxiety. More importantly, targeting accuracy is degraded, e.g. wing mounted missiles cannot be fired because of high levels of wing motion that prevent target lock-on.

As an example a recording is shown in figure 1 of LCO of a fighter aircraft which was encountered during flight flutter tests [1]. In many cases, as in figure 1, the maximum amplitudes occur during aircraft deceleration. LCO is experienced by aircraft with highly swept wings as well as with high aspect ratio wings, although different flow mechanisms may be involved. In references 2 to 6 such cases were analyzed in relation to wing bending oscillations.

For fighter aircraft, LCO is characterized by an almost harmonic oscillation which appears at Mach numbers ranging from 0.8 to 1.1, and at moderate angles-of-attack depending on the Mach number, but usually less then 10 deg. The flow conditions during LCO are characterized by mixed attached/separated flow. Lowly damped vibration modes tend to respond provided they have the proper characteristics to couple with this type of flow. This coupling frequently occurs near flutter boundaries, which implies that classical flutter predictions with linear theory may be applied as a guide for identifying lowly damped modes in the transonic speed range that might be sensitive to LCO.

Several research programs on unsteady aerodynamics and flutter predictions were conducted by NLR and General Dynamics to improve the accuracy and reduce the time and costs of flutter clearance of the many store configurations of a fighter aircraft. Currently there are several aerodynamic computer codes available to predict the unsteady loading in subsonic, transonic, and supersonic inviscid flow. However, codes capable of dealing with the transonic speed range with regions of separated flow and shock-wave/boundary-layer interactions have not yet been developed to an acceptable level of reliability.

In response to the above needs, an investigation was started as a cooperative effort between NLR and General Dynamics to understand the nature of LCO experienced by fighter

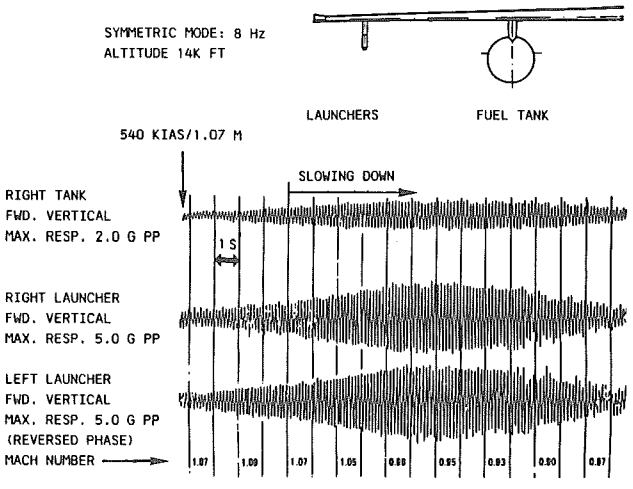

Fig. 1 Recordings of accelerometers during flight flutter testing of fighter-type aircraft.

aircraft maneuvering at transonic speeds. This investigation is being funded by the US Air Force, The Netherlands Ministry of Defense, General Dynamics, and NLR. In addition to conducting an extensive wind tunnel investigation [7,8,9], a major objective of this investigation is to develop a method for predicting LCO characteristics of full scale aircraft. The wind tunnel data from references 8 and 9 will be used in some form for guidance in the development of the method.

An analysis of steady wind tunnel data, obtained for a fighter type aircraft, has indicated that shock-induced and trailing-edge separation play a dominant role in the development of LCO at transonic speeds as first described in reference 10 and further discussed in reference 11. On the basis of these data a semi-empirical prediction method was developed. A preliminary version of this method and some results were presented in reference 12 and further developments were discussed in reference 13. As described in these presentations, the method has been applied to several configurations and has correctly identified those which have encountered LCO.

This paper will present further developments of the method aimed at improving the understanding of the nonlinear mechanisms involved with predicting transonic LCO. The basic method will first be reviewed including a summary of the conclusions reached in earlier presentations [13,14]. Next, a modified analytical model will be presented to include the importance of static aeroelastic effects in the LCO model. Finally, the implementation in the LCO model of a simple aerodynamic time lag concept as suggested in reference 8 and 9 will be compared with preliminary results of the experimental data analysis.

II. Basic LCO Prediction Method

A review of the method, including a modified model, will be given in this section. The nonlinear aerodynamics involved with transonic LCO will first be discussed followed by a description of the aeroelastic equations of motion and their solution using a time-marching approach.

II.1 Nonlinear Aerodynamics for LCO

In order to identify the important nonlinearities in the aerodynamic forces that could drive LCO, steady pressure data of a full-span wind tunnel model of a typical fighter aircraft were analyzed at NLR which were made available by the aircraft manufacturer [15]. The objective of that test was to obtain pressure data for investigating the role of shock-induced trailing-edge separation in LCO as suggested in reference 10. Pressure data were acquired on the wings, the horizontal tails and the fuselage for the following test conditions: Mach number ranging from 0.90 to 0.96, with increments of 0.01, and angle-of-attack ranging from 0 to 10 deg, with increments of 0.5 deg. During these tests different tip launchers and leading-edge flap settings were also included in the configuration matrix. The wing planform of the wind tunnel model provided with pressure orifices is shown in figure 2. Also shown is the panel distribution used in the chordwise and spanwise integration.

Results of the NLR analysis are presented for one type of tip launcher and one leading-edge flap setting. In figures 3 and 4 the steady normal force and moment section coefficients are shown for stations 1 and 6 (most inboard and outboard, respectively) as function of angle-of-attack (0 to 10 deg) and Mach number (0.90 to 0.96). The coefficients for the intermediate stations show a gradual transition. It is immediately clear that the coefficients in station 1 do not show any irregular behavior, whereas in station 6 both lift and moment coefficients show rapid changes in short intervals of the angles-of-attack (centered on about 5 to 7 deg) in the greater part of the Mach number interval. These rapid changes are typical of those described in reference 10 that were shown to drive LCO.

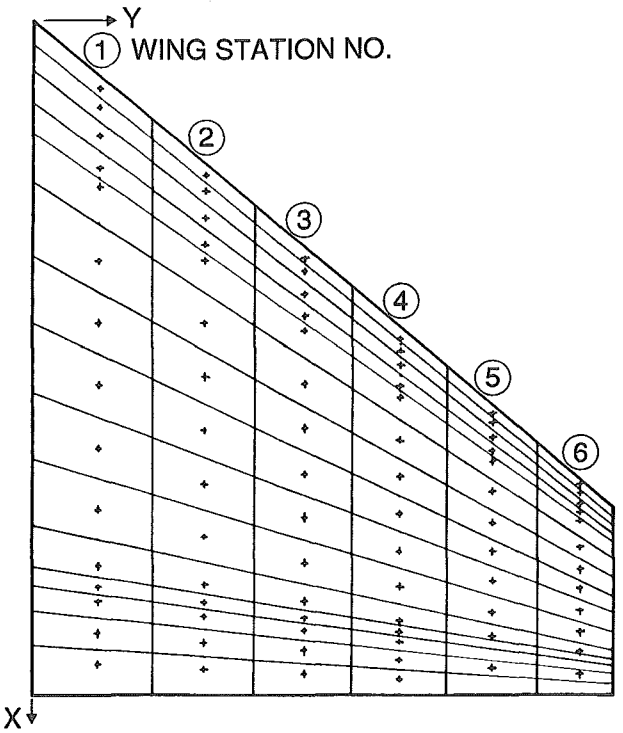

Fig. 2 Location of pressure orifices and corresponding panels on the model wing planform.

To analyze the kind of pressure distributions which lead to the rapid changes in the section aerodynamic coefficients, the pressure distributions on the upper and lower wing surface in stations 1 and 6 at Mach number 0.92 are presented in figures 5 and 6. The pressure distribution at the upper surface in station 1 shows a very gradual development with angle-of-attack, with a small upstream shift of the shock along with a slight trailing edge flow separation at the highest angle-of-attack. At station 6 a strong upstream shift of the shock starts at about 5 to 7 deg coupled with a rapidly developing flow separation at the trailing edge. This occurs after a merging of the weaker nose and aft shocks into a much stronger single shock that induces the extensive separation as is discussed in detail in reference 16. The shock motion also reverses at this point which coincides with breaks in the sectional lift and pitching moment coefficients. The pressure distributions on the lower side show only very gradual developments.

The observed characteristics of the section aerodynamic coef-

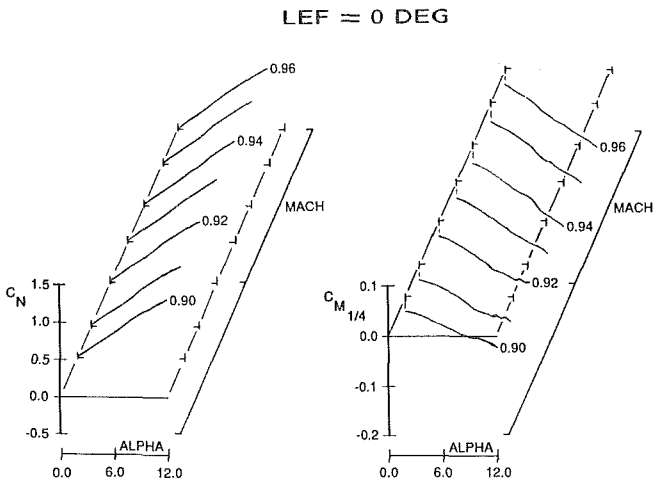

Fig. 3 Steady lift and moment coefficients at station 1 as function of Mach number and angle-of-attack.

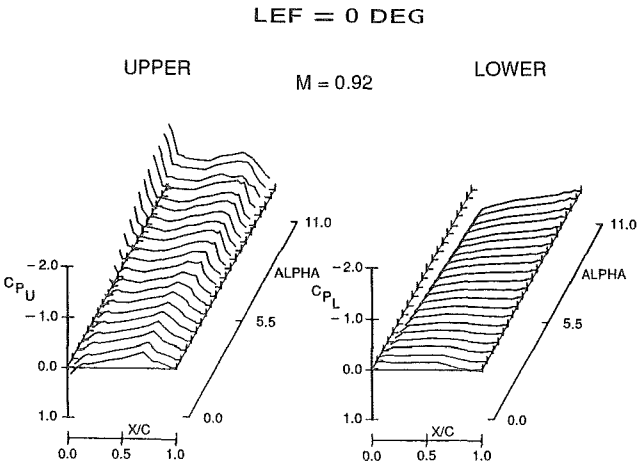

Fig. 5 Steady pressure distributions at station 1 as function of angle-of-attack and constant Mach number (M = 0.92).

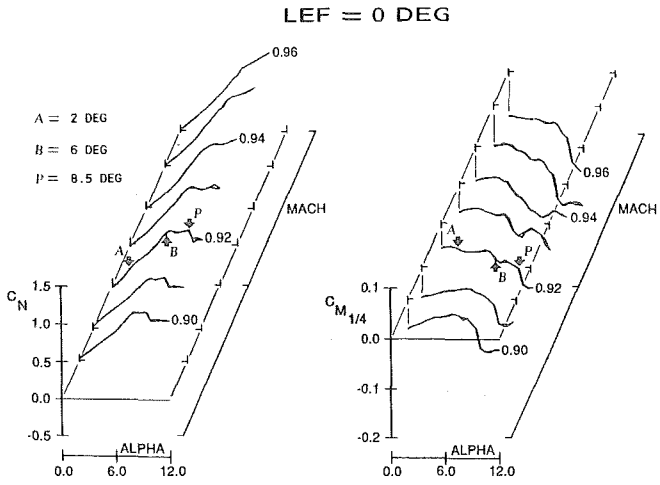

Fig. 4 Steady lift and moment coefficients at station 6 as function of Mach number and angle-of-attack.

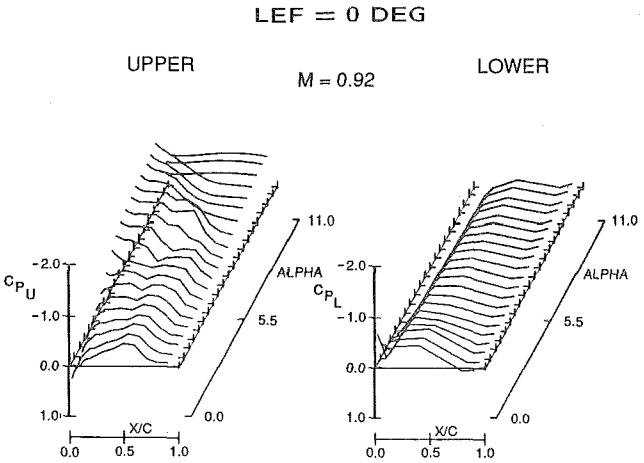

Fig. 6 Steady pressure distributions at station 6 as function of angle-of-attack and constant Mach number (M = 0.92).

ficients and pressure distributions on the upper wing surface in station 6 are shown more convinceble in figures 7 and 8. In figure 7 the quasi-steady section aerodynamic dirivatives at station 6 as function of Mach number and angle-of-attack are presented. Quasi-steady pressure distribution dirivatives at station 6 as function of angle-of-attack and constant Mach number (M = 0.92) are shown in figure 8. These quantities are of more interest to the discussion of unsteady data presented in reference 9. At low mean incidence, the pressures have a definite nose-up pitching moment characteristic, whereas at higher mean incidence, the characteristics has changed clearly to a nose-down pitching moment. The reversal of the shock oscillation peak is a result of the reversal of shock motion with increasing incidence as noted above for the steady data. The high suction levels aft of the shock are a result of the skock-induced separation reaching the trailing edge. Again the pressure distributions on the lower side show gradual developments. The observed typical characteristics correspond to the phenomena described in references 11 and 17.

For the other type of tip launcher and leading-edge flap settings the same kind of trends were observed.

II.2 Aeroelastic Equations of Motion

An adequate description of the displacements of the unrestrained aircraft structure is obtained by taking: 1) the flexibility matrix of the free-free aircraft structure to describe the static displacements and 2) a set of symmetric and antisymmetric natural vibration modes as generalized coordinates, completed by adding the rigid body modes. The equations for static displacements are expressed then in matrix form

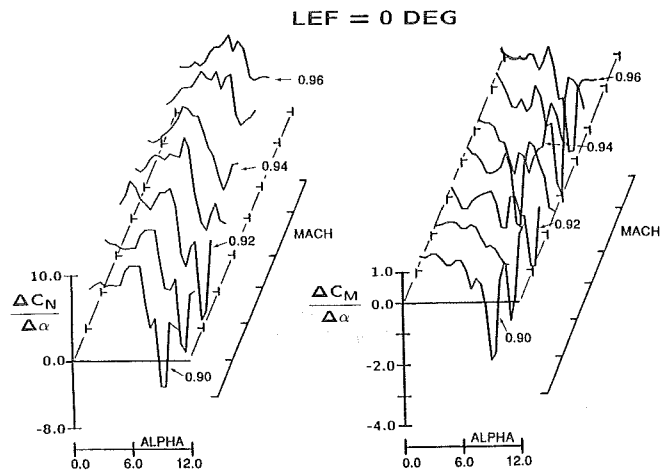

Fig. 7 Quasi-steady section lift and moment dirivatives at station 6 as function of Mach number and angle-of-attack.

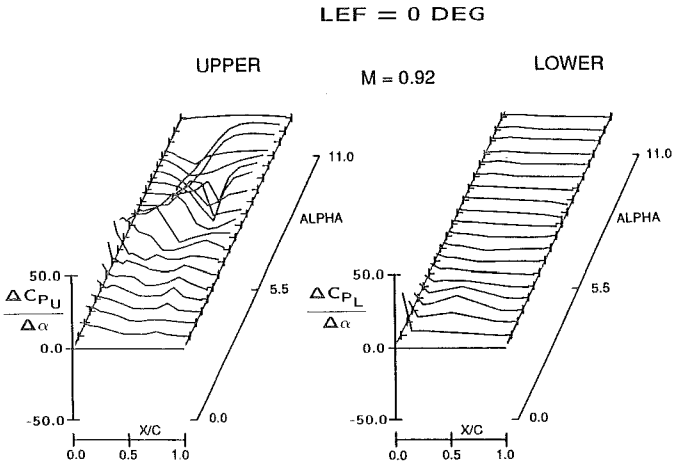

Fig. 8 Quasi-steady pressure distribution dirivatives at station 6 as function of angle-of-attack and constant Mach number (M = 0.92).

as:

$$\{h_m\} = [C_{FF}]\{F_a\} \tag{1}$$

where h_m is the vector of static displacements, C_{FF} is the "interpolated" flexibility matrix for the aerodynamic control points which is obtained from the flexibility matrix based on the structural control points, and F_a is the vector of mean aerodynamic loading. The equations of motion are expressed in matrix form as:

$$\begin{bmatrix} M_R & 0 \\ 0 & M_E \end{bmatrix} \begin{Bmatrix} \ddot{q}_R \\ \ddot{q}_E \end{Bmatrix} + \begin{bmatrix} 0 & 0 \\ 0 & 2\zeta_E M_E \omega_E \end{bmatrix} \begin{Bmatrix} \dot{q}_R \\ \dot{q}_E \end{Bmatrix} + \begin{bmatrix} 0 & 0 \\ 0 & M_E \omega_E^2 \end{bmatrix} \begin{Bmatrix} q_R \\ q_E \end{Bmatrix} = \begin{Bmatrix} L_R \\ L_E \end{Bmatrix}, \tag{2}$$

where M is the generalized mass matrix and q is the vector of generalized coordinates. The indices R and E refer to the rigid body and elastic modes and their number is N_R and N_E , respectively. ζ and ω are the damping factor and natural frequency of each elastic mode. L_i is the generalized aerodynamic force for the i-th coordinate.

The mean aerodynamic load distribution F_a is formulated as:

$$F_a = \frac{1}{2}\rho V^2 \int_{\Delta S} C_p^s\langle x, y, \alpha_s\rangle dS, \tag{3}$$

in which $\frac{1}{2}\rho V^2$ is the dynamic pressure, $C_p^s\langle x, y, \alpha_s\rangle$ is the pressure distribution over the wing depending on the angle-of-attack distribution α_s, and ΔS is the panel area.

The generalized aerodynamic force for the i-th coordinate, L_i, is defined as:

$$L_i = \frac{1}{2}\rho V^2 \int_S \phi_i\langle x, y\rangle C_p^*\langle x, y, \alpha\langle t\rangle\rangle dS, \tag{4}$$

where $\phi_i\langle x, y\rangle$ is the natural mode shape and $C_p^*\langle x, y, \alpha\langle t\rangle\rangle$ is the differential pressure distribution over the wing,

$$C_p^*\langle x, y, \alpha\langle t\rangle\rangle = C_p\langle x, y, \alpha\langle t\rangle\rangle - C_p^s\langle x, y, \alpha_s\rangle \tag{5}$$

depending on the angle-of-attack distribution α. This distribution is expressed by:

$$\alpha = \alpha_s + \Delta\alpha, \tag{6}$$

$$\alpha_s = \alpha_m + \frac{\partial}{\partial x} h_m, \tag{7}$$

$$\Delta\alpha = \sum_{N_R+N_E} \left(\frac{\partial}{\partial x} + \frac{1}{V}\frac{\partial}{\partial t}\right) \phi_j\langle x, y\rangle q_j\langle t\rangle. \tag{8}$$

α_m is the prescribed angle-of-attack, and $\Delta\alpha$ the time-dependent variation at point x, y. In the present approach the pressure distribution C_p in expressions (3) to (5) is a time-independent nonlinear function of α. It is the relation (4) by which the aerodynamic peculiarities discussed in section 2.1 enter the equations of motion (2), weighted by an appropriate mode shape ϕ_i.

In the numerical solution of the equations of motion the aerodynamic forces F_a and L_i are discretized as follows:

$$F_a^k = \frac{1}{2}\rho V^2 \left(C_p^s\langle x, y, \alpha_s\rangle\right)_k \Delta S_k, \tag{9}$$

and

$$L_i = \frac{1}{2}\rho V^2 \sum_k \left(\phi_i\langle x, y\rangle C_p^*\langle x, y, \alpha\langle t\rangle\rangle\right)_k \Delta S_k, \tag{10}$$

in which ΔS_k is the k-th panel area, and $\langle C_p^s\rangle$ in expression (9) and the product $\langle \phi_i C_p^*\rangle$ in expression (10) are taken constant over the whole k-th panel, being evaluated at the $\langle x, y\rangle$ position of the k-th pressure orifice. Because of the nonlinear aerodynamics, these forces have to be evaluated for both right and left wing and added correctly at each time step of the time simulation. It should be noted that in the present study only aerodynamic forces on the wing have been taken into account and those on the wing stores, fuselage and empennage surfaces ignored.

Before solving, the complete set of equations of motion (1) and (2), the expression (2) are brought into state space form. Writing equation (2) as:

$$[M]\{\ddot{q}\} + [C]\{\dot{q}\} + [K]\{q\} = \{L\langle q, \dot{q}\rangle\}, \tag{11}$$

their state space form is:

$$\{\dot{s}\} = [M]^{-1}\left(\{L\langle q,\dot{q}\rangle\} - [C]\{s\} - [K]\{q\}\right), \qquad (12)$$

$$\{\dot{q}\} = \{s\},$$

and the working form is:

$$\{\dot{x}\} = [A]\{x\} + [B]\{u\}, \qquad (13)$$

where A and B are constant matrices that result from the change of the variables $x = [s,q]^T$ and u is the generalized force $L\langle q,\dot{q}\rangle$.

The influence of static deformation enters the calculations through a simply iterative matrix multiplication (1). When the static deformations are within an assigned accurancy the dynamic part of the calculations is started.

The aeroelastic time-marching solution procedure applied to integrating equation (13) is similar to that described by Edwards et al [18]. Details of this procedure are given in references 13 and 14. The final result of the time integration process is the variation of the generalized coordinates q and their time derivatives as functions of time.
They can easily be reduced to quantities of practical interest, like wing tip acceleration, pilot seat acceleration, etc.

III. Previous Results

Previous studies of the LCO prediction method were reported in references 13 and 14. The formulation of the aeroelastic equations of motion was slightly different and did not include the representation of static aeroelastic effects. Many applications were made to both generic as well as realistic configurations. In addition to various parametric effects, the basic mechanism of coupling between flow fields and structural response was examined for the generic model. Predictions were also made for realistic configurations, some of which were known to exihibit LCO and others that did not. The results of both references so far as relevant for the present paper are summarized below.

III.1 Results of Reference 13

The main result was that the data from steady wind tunnel tests given in reference 15 were sufficient for predicting the essential features of LCO. This may be confirmed here by figure 9 in which for configuration A LCO acceleration responses are shown at different values of the structural damping g. The LCO responses, however, are too large even for g = 0.03, as compared with the response level of 3g to 5g being known from flight tests. It turned out that this level could be obtained by increasing the structural damping values to about g = 0.05.

In all cases two natural modes of the aircraft structure were dominant in the development of LCO as are shown in figure 10. Both vibration modes show similar torsional deflections of the outer wing parts, but their bending deflections are opposite. During LCO they couple in a classic flutter where one coupled mode becomes unstable, but at a limited amplitude since the aerodynamic forces are now highly non-

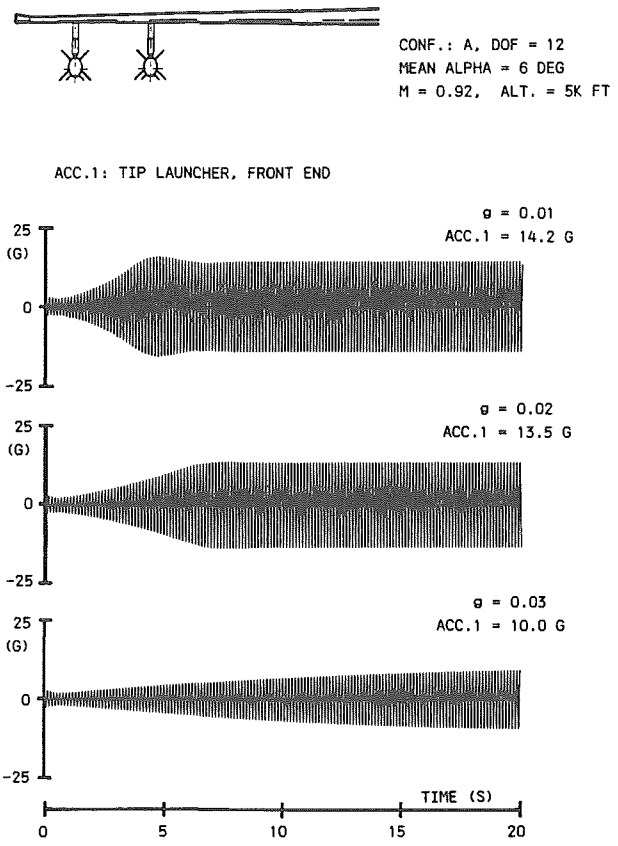

Fig. 9 Response calculation of Conf. A; 12 DOF, M = 0.92, α_m = 6 deg, alt. = 5K ft, structural damping variable.

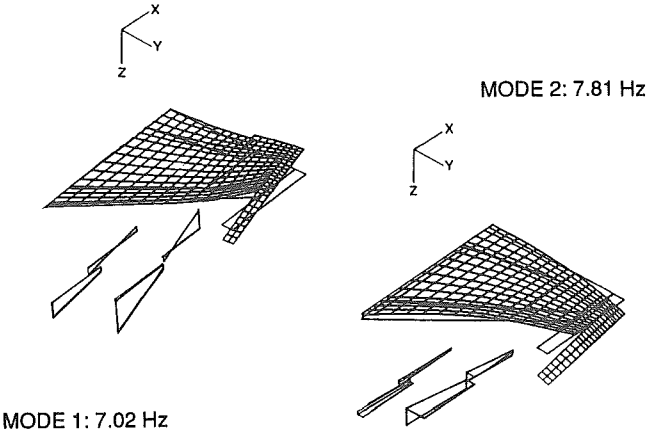

Fig. 10 First two unrestrained vibration modes of generic model.

linear.

The potential role of shock-induced trailing-edge separation during LCO was also demonstrated. The wing motion and the pressure distributions on the upper surface are shown in figure 11 for one cycle of oscillation for an LCO calculation. The cycle starts at 25.1 s and the time intervals are 0.005 s. The time values during the cycle were chosen to highlight

the incremental angle-of-attack for (I) maximum nose down, (II) zero with positive pitch rate, (III) maximum nose up, and (IV) zero with negative pitch rate.

The results in figure 11 may be used to clearly demonstrate the relationship between shock-induced trailing-edge separation and LCO. At point I in figure 11, the wing tip is at a minimum total angle-of-attack (i.e. $\alpha = \alpha_m + \Delta\alpha$) of about $\alpha = 4.7$ deg and a large positive (up) deflection as indicated by the deflections (heavy line) at station 6. Two shocks (nose and aft shocks) are distinctly seen in the chordwise pressure distributions (heavy line) also at station 6. The flow is attached at the trailing edge as indicated by the nearly zero value of the pressure coefficient. C_N is at its lowest value during the cycle and C_m is at its highest (nose up) value. Thus, attached flow with two shocks is providing a nose up pitching moment increment at the minimum angle and a downward acting normal force incremental at a large upward deflection.

Continuing on to point II in figure 11, the wing tip is at $\alpha = 6$ deg and a maximum downward deflection. The two shocks have merged into a single strong shock and the trailing edge pressures are indicating that separation has begun. C_N is higher but C_m is lower (less nose up).

At point III in figure 11, the wing tip is at a maximum angle-of-attack of about $\alpha = 7.3$ deg. The single strong shock formed at point II has fully separated the flow to the trailing edge which in turn has driven the shock forward as shown in the pressures at station 6. C_N is still about the same as it was at point II, however, C_m is now lower and more nose down.

Finally, at point IV in figure 11, the wing tip is at about $\alpha = 6$ deg but maximum upward deflection. The trailing edge pressures are indicating that re-attachment is occurring and a strong single aft shock is now present. C_N is the same as it was at $\alpha = 7.3$ deg at point III but C_m is higher giving less nose down pitching moment. From point IV, the cycle continues to point I where the two-shock system is reformed.

The relationship just illustrated between shock-induced trailing-edge separation, pitching moment and torsion response at station 6, is identical to that described in reference 10 where it was concluded that a nonlinear aerodynamic spring was the principal driving mechanism for LCO. For the current example, however, significant vertical translation in the LCO (or eigen) mode was opposed by C_N variations at point II. For angles-of-attack above $\alpha = 6$ deg , C_N was constant and did not affect the wing motion which would make it a neutral spring for half of the cycle. Thus, the existence of an additional nonlinear spring for opposing translation for half of the cycle further substantiates the above conclusion of reference 10.

In addition to the above demonstration of the mechanism

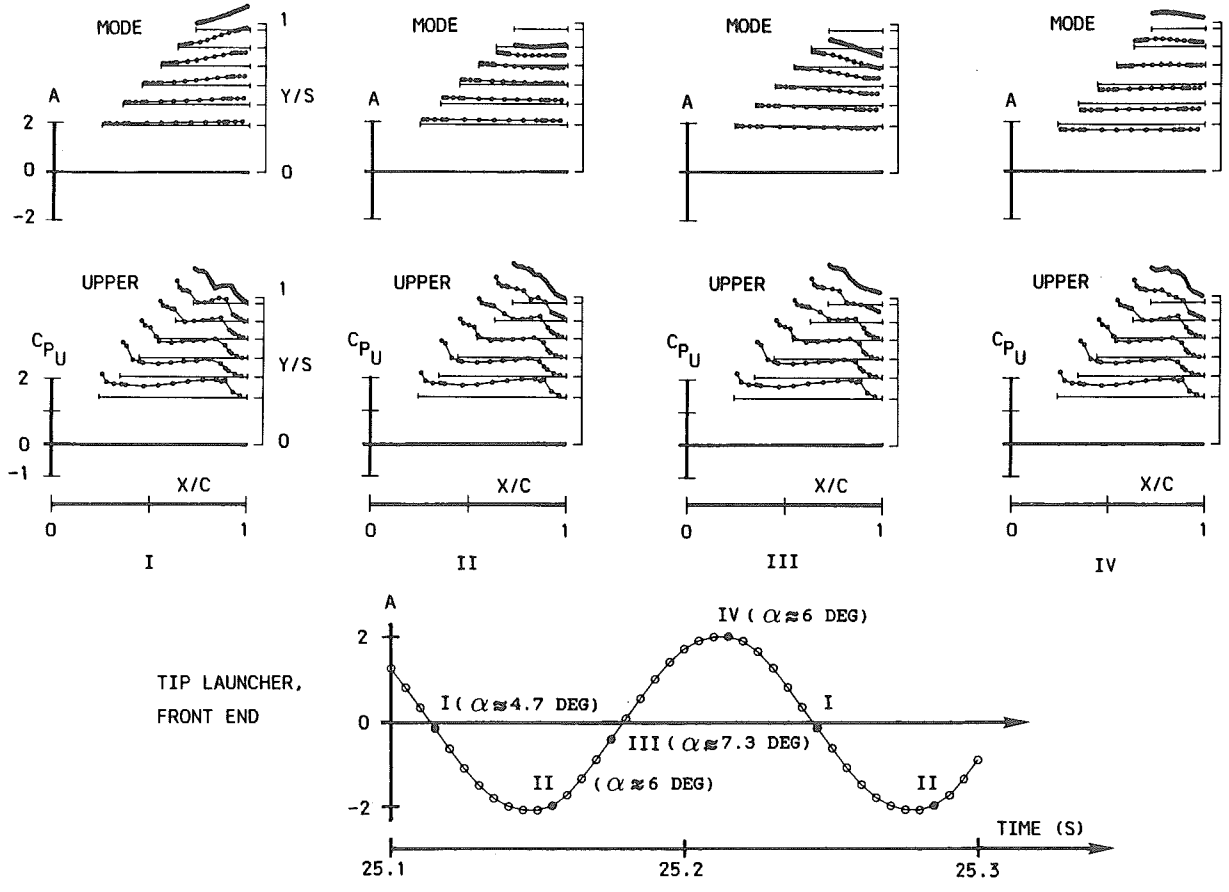

Fig. 11 Vibration mode and flow characteristics for generic model during LCO.

which can produce LCO, the effects of altitude, mean angle-of-attack and total damping were found to be of first order importance. The predicted effects of wing store configurations on LCO trends were also shown to agree qualitatively with known characteristics of the considered configurations.

In conclusion, the potential of the method was demonstrated to provide qualitatively correct predictions of LCO. which could make the method an effective tool for application early in the design process of new aircraft. However, it was also realized that further refinements were necessay.

III.2 Results of Reference 14

The parametric study reported in reference 13 was continued, and results of it were presented in reference 14. The unsteady wind tunnel test had just been completed, but no unsteady data were available for incorporation into the prediction method.

Leading-edge flap setting was considered to be an important parameter for the predictions. In addition to data for zero leading-edge flap deflection, data for two other positions of 5 deg and 10 deg (nose down) are available in the data base of reference 15. The effect of leading-edge flap settings was investigated with the LCO prediction method by substituting pressure data for the flap setting of interest and running the method in its normal mode.

The results in figure 12 indicate that leading-edge flap settings have a significant effect on LCO development during a simulated maneuver. The levels of LCO for leading-edge flaps at 0 deg and 5 deg are low at ±3 g's. However, normal flying practice with optimized leading-edge flap scheduling, depending on Mach number and altitude, might tipically use 0 deg flap up to about 2 deg angle-of-attack, 5 deg flap at about 6 deg, and 10 deg flap at about 8 deg. With such scheduling, the heavy LCO shown in figure 12 for 10 deg flap would not be encountered since this flap setting would not be used below about 7 or 8 deg angle-of-attack. Corresponding points for the other leading-edge flap settings of 0 deg and 5 deg would encounter the milder LCO shown for these points.

Additional major topic was the examination of effects that parameters in the aerodynamic modeling for representing unsteady characteristics, would have on the development of LCO.

The first parameter was an aerodynamic time lag. It was reasoned that some time is required for the flow to separate or reattach, and that therefore a time lag had to be introduced into the quasi-steady aerodynamic forces used in the prediction method. From several sources of unsteady flow information the existence of a more or less "universal" time lag was proposed in references 8 and 9, defined as:

$$\Delta\tau_{LAG} = \frac{2V\Delta t_{LAG}}{c_{SEP}} \approx 8.4,$$

where c_{SEP} is the approximate chord length of the shock-induced trailing-edge separation zone (or the mean distance from the shock to the trailing edge). For the LCO model considered this value corresponded to an estimated physical value of $\Delta t_{LAG} = 0.011$ seconds or a phase lag of about

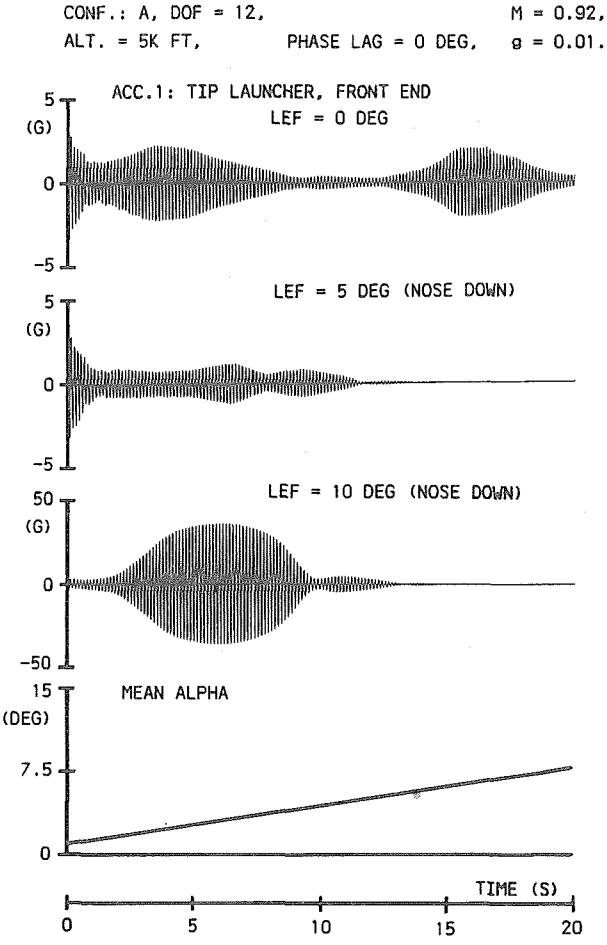

Fig. 12 Calculated response variation with leading edge flap deflections of Conf. A; 12 DOF, M = 0.92, α_m variable, alt. = 5K ft, structural damping: g = 0.01, phase lag = 0 deg.

30 deg at 7.6 Hz.

A variable phase lag was introduced into the prediction method, being uniformly valid for all generalized aerodynamic forces. Surprisingly, application of a phase angle of 30 deg for configuration A resulted in an unstable motion, and only by increasing the structural damping to g = 0.05 a stable LCO was achieved. This is shown in figure 13, and the need of increasing the structural damping becomes immediately apparant after comparison with figure 9. The structural damping has now to be considered as a total damping, i.e. as the sum of the true structural damping (g ≈ 0.02) and aerodynamic damping. This total damping was another important parameter in reference 14.
Variation of the phase lag showed that stable LCO with realistic amplitudes and structural damping values (g = 0.02) could only be found for negative phase lag, i.e. phase lead with angles between 0 and 45 deg. This is shown in figure 14.

A different view was taken by fixing the phase angle on 30 deg and varying separately the total damping values of the critical modes 1 and 2 (see figure 10) as needed to obtain stable LCO. Different values were found, leading to the conclusion

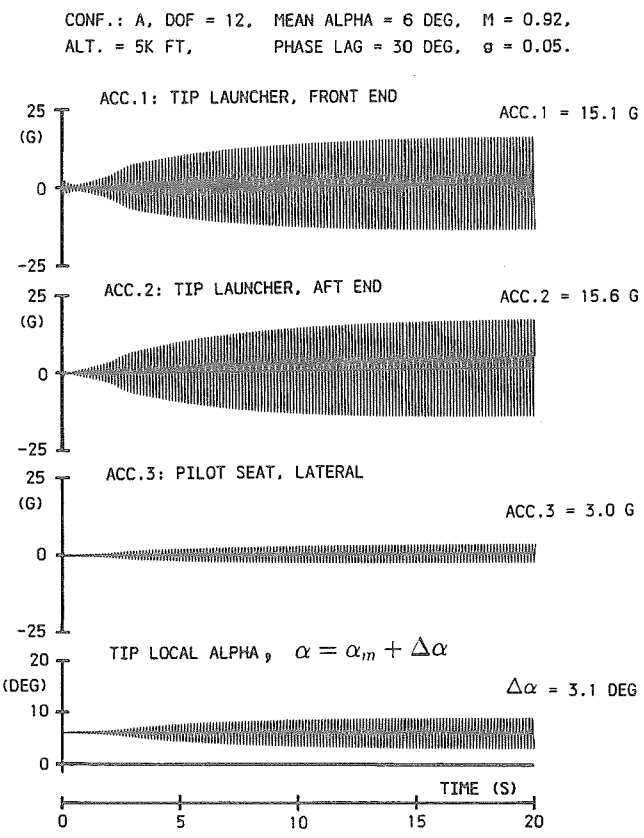

Fig. 13 Response calculation of Conf. A; 12 DOF, M = 0.92, α_m = 6 deg, alt. = 5K ft, structural damping: g = 0.05, phase lag = 30 deg.

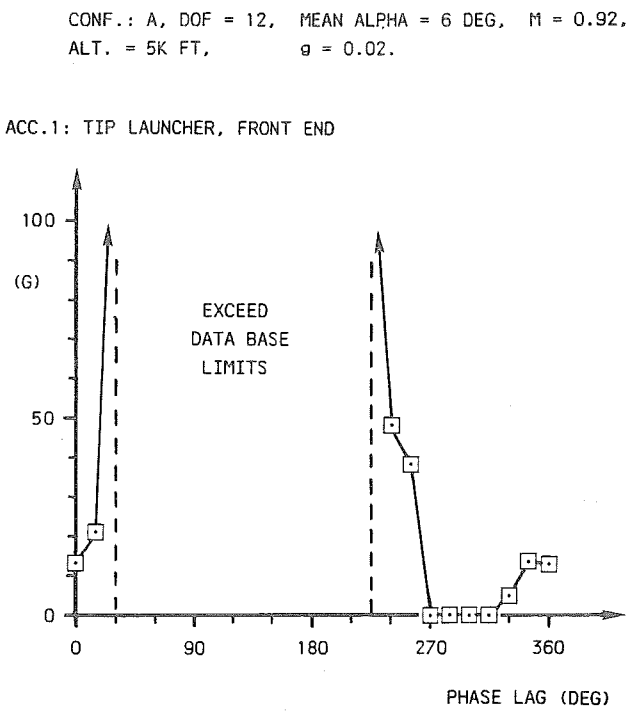

Fig. 14 Calculated response variation with time lag of Conf. A; 12 DOF, M = 0.92, α_m = 6 deg, alt. = 5K ft, structural damping: g = 0.02.

that total damping values for the critical modes should be made mode dependent in order to establish the correct LCO characteristics.

It was realized from the beginning that a "universal" time lag could only provide a very crude and possible hardly acceptable description of the unsteady effects in the aerodynamic modeling. However, the purpose of investigating this simple model was to determine the importance of time lag effects in the prediction of LCO. With the experience of applying the "universal" time lag as described before, the need immediately became evident to improve and refine the description. One could then think of a differentiation between phase angles for attached flow (wing lower side and inner part of the upper side, and at low angles-of-attack) and separated flow (outer part of the wing upper side at higher angles of attack). Even varying phase angles in these regions could be considered. It seems obvious, however, that such adaptations of the aerodynamic modeling can only be performed after a profound analysis of the unsteady wind tunnel test data [9].
Awaiting the results of this analysis the steps have been taken recently as described in the following sections.

IV. Static Aeroelastic Effects

An item of great importance has turned out to be the introduction of static aeroelastic effects into the LCO model. Since the transonic shock-induced separated flows are highly sensitive to local static changes in mean angle-of-attack, it is important that these effects be accounted for. This aspect was discussed in reference 13 where the use of modal residualization was suggested as a means to account for higher frequency modes not included in the dynamic simulation but which could be important in the static aeroelastic effects.

Given the fact that only pressure distributions over the wing surface are available a different approach to investigate the static aeroelastic effects has been chosen. The LCO model was modified (see section 2.2) to allow that 1) mean aerodynamic loading and an adapted aeroelastic flexibility matrix of the aircraft structure may be applied to determine the static deformation, 2) a complete set of symmetrical and antisymmetrical modes up to frequencies of interest, including rigid body modes may be used to simulate the dynamic effects. The differential between the instantaneous aerodynamic loading and mean aerodynamic loading are applied as driving forces in the equations of motion (see section 2.2).

The original formulation of the model could simulate cases for a mean angle-of-attack only with the contributions of antisymmetrical vibration modes. The modified LCO model now has the capability to include both symmetrical and/or antisymmetrical vibration modes, because the generalized forces in the equations of motion are defined for the differential aerodynamic loading.

In order to demonstrate the effects of static aeroelasticity, response calculations were made for configuration A at the

same conditions as presented earlier in figures 9. Results will be shown for a system with symmetrical and antisymmetrical natural modes up to 15 Hz (23 DOF, 11 symmetric and 12 antisymmetric modes). Next, the influence of static deformation will be shown. In addition, the section coefficients at the wing tip station 6, will be presented that occur during the LCO calculations.

In figure 15 the results are presented for configuration A at the same conditions noted in figure 9. The upper part of the figure shows the responses without static deformation of the forward tip launcher accelerations and the local dynamic angle-of-attack. The acceleration levels are about the same as shown earlier in figure 9 for the same conditions and essentially represent an antisymmetrical LCO at 7.5 Hz. Note the slight differences in response levels up and down, which is caused by a symmetrical mode at a frequency close to 15 Hz (about twice the frequency of the LCO mode).
The lower part of the figure shows the results including static deformation. It appears that the static deformation has a large reducing effect on the response levels, which is caused by a static nose-down angle-of-attack change near the wing tip area.
Without the simulation of the symmetrical modes, the response levels appeared to be slightly higher in this case.

Instantaneous sectional lift and moment coefficients for the wing tip station, which correspond to the results of figure 15 are shown in figure 16. In this figure the hysteresis loops of the section coefficients during LCO and the steady coefficients (as insets) for the same condition as shown in figure 4 are presented. The hysteresis of the loops is largely caused by the time-derivative shown in Eq. (8) of section 2.2. Without static deformation, the curvature of the hysteresis loops corresponds to the curves in steady lift and moment coefficients between the indicated points 3 and 5. It is clearly shown that the moment coefficient represents a destabilizing hysteresis loop (clockwise) which corresponds with the negative slope of the moment coefficient steady curve for the indicated part. The hysteresis loops at station 5 (Fig. 2) present the same character.
Taking into account static deformation leads to much smaller hysteresis loops of lift and moment coefficients for the wing tip station. Even the orientation of the loops is changed (counter-clockwise). The curvature of the loops correspond to the curves of the steady coefficients between the indicated points 2 and 4 which is at a lower mean angle-of-attack caused by the static deformation. The moment coefficient in this section now shows a stabilizing character (positive damping). In this case the the aerodynamics (not shown) present in stations 4 and 5 (Fig. 2) are responsible for driving the LCO. For the current results in which no aerodynamic time lag is considered, the conclusion is that the change of the aerodynamic behavior due to static deformation contributes to a reduction of the response levels during LCO. For a realistic simulation, however, also the effect of an aerodynamic time lag should be included.

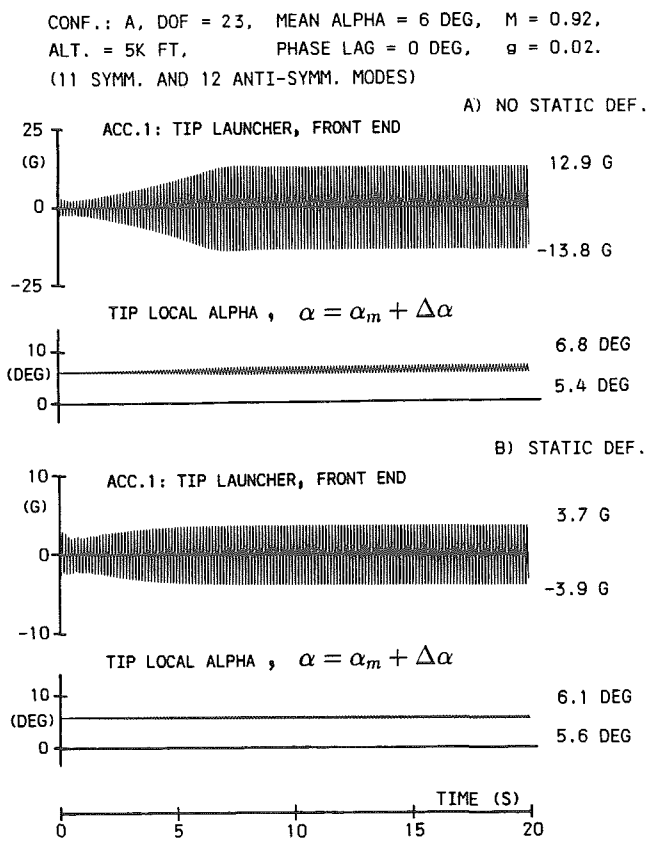

Fig. 15 Response calculation of Conf. A; 23 DOF, M = 0.92, α_m = 6 deg, alt. = 5K ft, structural damping: g = 0.02, phase lag = 0 deg, (Influence static deformation).

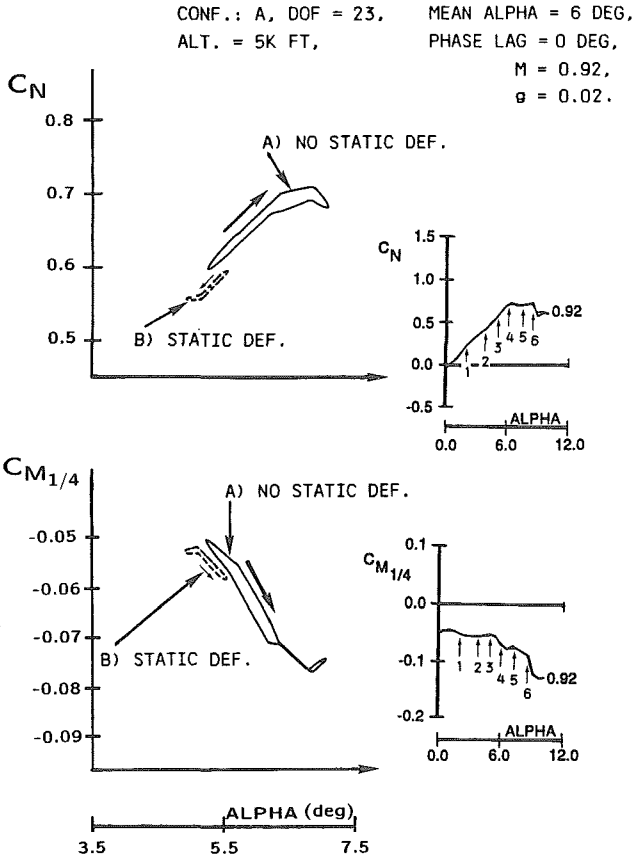

Fig. 16 Lift and moment section coefficients in wing station 6 as function of local angle-of-attack.

V. Aerodynamic Time Lag Concept

In figures 17 to 20 the applied aerodynamic time lag concept in the LCO model as suggested in reference 9 is verified with preliminary results of a wind tunnel investigation of an harmonically oscillating fighter type wing [9]. Hysteresis loops of the oscillatory time histories of lift and moment section coefficients are shown for various mean incidences and compared with the mean value curves at station 6 for Mach numbers 0.90 and 0.93 in figures 17 and 18, respectively. The directions in which the loops are passed are indicated for both Mach numbers. It appears that for both Mach numbers the direction of the lift coefficient loops is counter-clockwise for mean incidences up to 6.5 deg and becomes clockwise for incidences from 6.5 deg on.

The moment coefficients for M = 0.90 are characterized by counter-clockwise loops for incidences up to 4 deg (positive damping), and by clockwise loops from 4 deg up to 8 deg (negative damping) (Fig. 17). For M = 0.93 the same character is present, except for the incidence at 7 deg where the orientation of the loop is changed to counter-clockwise (positive damping). The moment coefficient loops appear to track clearly the slopes of the mean value curves. Negative slopes show a counter-clokwise loop and positive slopes a clockwise loop. The observed trends of lift and moment coefficients are similar to the investigation presented in reference 19.

By comparing figure 16 with figure 17 and 18 it is shown that indeed the direction of the hysteresis loops around 5 to 6 deg in figures 17 and 18 correspond to those in figure 16. This seems to validate the use of the phase lag angle of 30 deg in combination with the increased total damping to represent unsteady aerodynamic effects in the prediction method.

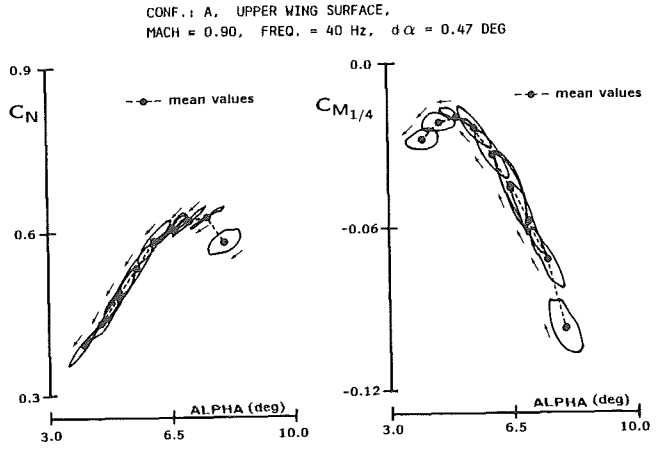

Fig. 17 Lift and moment section coefficients in wing station 6 as function of angle-of-attack (M = 90).

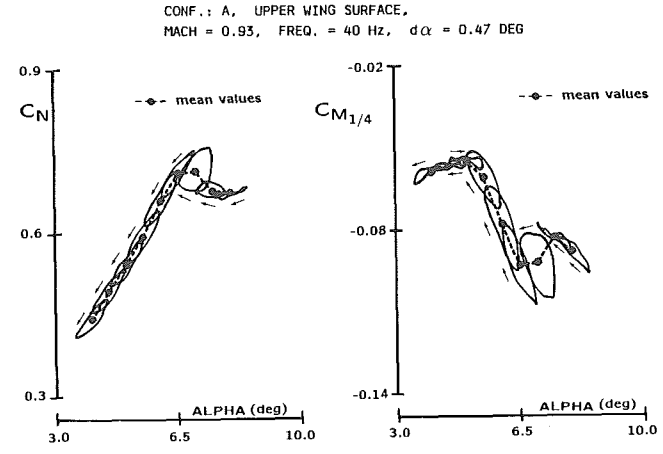

Fig. 18 Lift and moment section coefficients in wing station 6 as function of angle-of-attack (M = 93).

The results shown in figures 19 illustrate the variation of time lag with angle-of-attack for both C_N and C_m at wing stations 5 and 6 for Mach number 0.93. This time lag is derived from the estimated phase angles needed to match the unsteady C_N and C_m data with the mean value curves. As an example in figure 18, unsteady hysteresis loops for C_N between $\alpha = 4$ deg and 6.5 deg provide a $\Delta\alpha_{LAG}$ as defined by the horizontal width of the envelope of the hysteresis loops. This $\Delta\alpha_{LAG}$ is used to calculate a phase lag relative to the oscillatory wing motion amplitude of $d\alpha = 0.47$ deg. The phase lag is then converted into a Δt_{LAG} value.

The time lag in the wing station 5 for C_N data in figure 19 is about constant at 0.0017 s which corresponds to about 0.015 s full-scale. This value is reasonably close to the assumed value of 0.011 s used in the LCO calculations for a constant phase lag of 30 deg. The C_m data, however, indicate a higher average lag time of about 0.0028 s with an excursion to 0.0040 s at $\alpha = 6.5$ deg. A similar trend is noted in the wing station 6 data in figure 19 with a much greater excursion for both C_N and C_m at $\alpha = 7$ deg. In this station, the differences between C_N and C_m time lag characteristics are much less than at station 5. However, in both stations, the C_N time lag is about constant at 0.0017 s (with exception of $\alpha = 7$ deg in station 6).

The differences between the time lags for C_N and C_m data noted in figure 19 lead to the expected conclusion that a constant lag time value is not applicable over the entire wing. Thus, an examination was made of the chordwise variation of lag time for individual pressure measurements in wing station 5 and 6 for which the results are shown in figure 20. The station 5 time lag data were obtained at $\alpha = 7$ deg and the

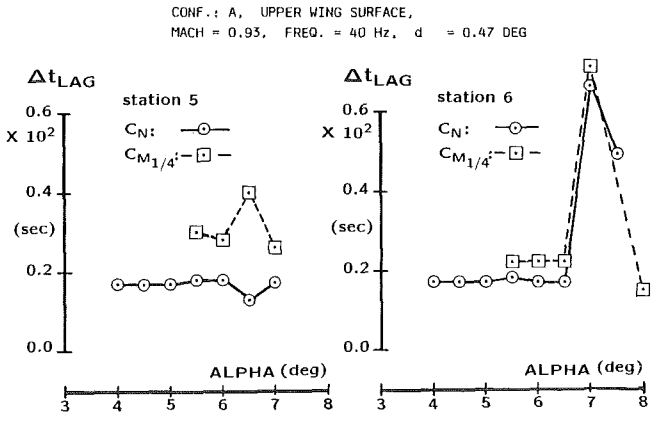

Fig. 19 Aerodynamic time lag of lift and moment section coefficients in wing stations 5 and 6 as function of angle-of-attack (M = 93).

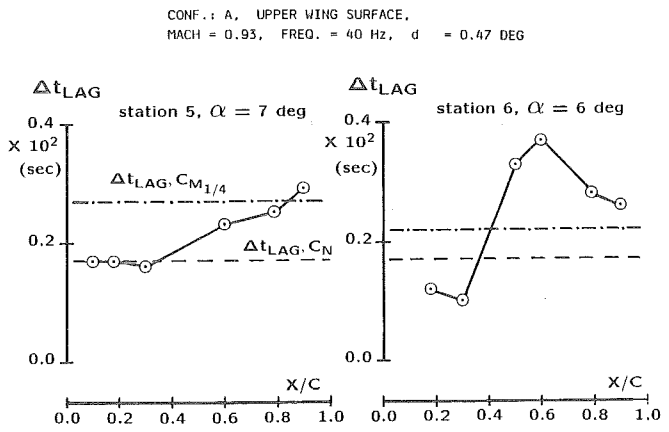

Fig. 20 Aerodynamic time lag of pressures in wing stations 5 and 6 as function of chordwise position (M = 93).

station 6 data at $\alpha = 6$ deg. These results were estimated on the basis of the pseudo phase angle relationship between the imaginary part of the first harmonic unsteady data and the slope of the mean C_p curve with respect to α. Also noted with the stations 5 and 6 results are the station lag times (dashed lines) for C_N and C_m as taken from figure 19 for the appropriate α values.

As can be seen in figure 20, there is considerable variation of time lag with chordwise and spanwise position. However, in both stations, the average C_N and C_m time lag values are within the range of the C_p time lag variations. These trends seem reasonable since lift is dominated by the forward pressures and moment is heavily influenced by the aft pressures. Thus, time lag for moment is more characteristics of the higher time lag values on the aft half of the two stations.

The above time lag analysis was approximate; however, further analysis is continuing with the aim to modify the time lag model so as to permit variation for each pressure orifice as a function of local flow conditions. Although this development will make the prediction method more complicated, the aim is still to retain computational simplicity but yet account for the major unsteady effects in obtaining unsteady airloads from steady pressure measurements.

VI. Method Refinements

Various refinements to the LCO prediction method were discussed in reference 13 which reflected the evolutionary development of such an approach. One of the key ingredients in the developments listed were the results from a recent unsteady wind tunnel test which is described in reference 9. The results discussed in section 3, 4 and 5 in this current paper were obtained as part of the investigation to better understand more specifically what information is needed from the unsteady wind tunnel test. These requirements are discussed in reference 9 but are summarized below along with a summary of the refinements suggested in reference 13.

The wind tunnel data base [9] is expected to provide information necessary to characterize the unsteady nature of three-dimensional transonic flows with extensive shock-induced separations that may also extend to the trailing edge. This information will provide the unsteady complement to that contained in reference 16. Such items of interest are flow transition lag times, effects of surface motion as well as the development of aerodynamic stiffness and damping forces. Information is also needed to determine if techniques such as those described in references 20 to 23 are capable of providing the unsteady aerodynamic loads suitable for use in the simulation of LCO phenomena.

The trends summarized in section 3 emphasize (1) the importance of accurately defining the unsteady aerodynamic characteristics in LCO flows and (2) the need for a generalized model of these characteristics that does not require condition dependent adjustments to match known results. This means that aerodynamic stiffness and damping forces in each natural mode used in the simulation must be known a priori through the use of some type of prediction technique which may be semi-empirical [20to23] or theoretical [24,25]. Current thinking suggests that configuration and condition specific information can be obtained from steady pressure tests (as is done for the current LCO prediction method) and that unsteady information can be developed that is more generic (such as transition lag time, etc.).

Finally, the use of aerodynamic forces on the fuselage and tail surfaces has also been considered in reference 13. Although these are important in buffeting and gust response predictions [26] they are probably not key ingredients to the LCO mechanism and may not be needed. However, this is still under consideration.

VII. Conclusions

A semi-empirical method to predict LCO characteristics of fighter aircraft is being developed. The method has been described in its present form, and results of the latest predictions were used to further assess various parametric effects. In addition to the conclusions in references 13 and 14, additional conclusions from the investigations discussed in the current paper are summarized below.

1. It appears that static deformations have a significant effect on response levels during LCO.
2. An analysis of some preliminary results of an unsteady wind tunnel test has shown that the simple time lag model applied in the LCO model has certainly a potential, but that further refinements of the model are necessary.

Acknowledgement

This investigation was funded by U.S. Air Force, General Dynamics, The Netherlands Ministry of Defense and National Aerospace Laboratory NLR, The Netherlands. The monitors for the USAF were: Messrs. Faustino Zapata and Larry Huttsell. The monitor for The Netherlands Ministry of Defense was the Netherlands Agency for Aerospace Programs (NIVR), contract number 07801N.

References

1. Meijer, J.J., "NLR Contributions to the Flutter Certification of Aircraft with External Stores", 7th Aircraft/Stores Compatibility Symposium, Wright-Patterson AFB, Ohio, 8-10 April 1986 and at the 17th Annual Symp. of the Society of Flight Test Engineers, Washington, D.C., USA, 10-14 August 1986.
2. Ericsson, L.E., "Vortex-induced Bending Oscillation of a Swept Wing", J. Aircraft, Vol. 24, No. 3, March 1987, pp. 195-202.
3. Dobbs, S.K., Miller, G.D., Stevenson, J.R., "Self Induced Oscillation Wind Tunnel Test of a Variable Sweep Wing", AIAA-85-0739, August 1985.
4. Moss, G.F., Pierce, D. "The Dynamic Response of Wings in Torsion at High Subsonic Speeds", AGARD-CP-226, 1977.
5. Seidel. D.A., Eckstrom. C.V., Sandford, M.C., "Investigation of Transonic Region of High Dynamic Response Encountered on an Elastic Supercritical Wing", AIAA-87-0735-CP, April 1987.
6. Eckstrom. C.V., Seidel. D.A., Sandford, M.C., "Unsteady pressure and structural Response Measurements on an Elastic Supercritical Wing", AIAA-88-2277.
7. Boer, R.G. den, Cunningham, Jr., A.M. "Unsteady Transonic Wind Tunnel Testing of Fighter Type Wings", 31st AIAA/ASME/ASCE/AHS/ASC SDM Conference, Long Beach, California, April 2-4, 1990.
8. Cunningham, Jr., A.M., Boer, R.G. den, "Transonic Wind Tunnel Investigation of Limit Cycle Oscillations on Fighter Type Wings", AGARD SMP Specialist Meeting on Transonic Unsteady Aerodynamics and Aeroelasticity, San Diego, California, 9-11 October 1991.
9. Cunningham, Jr., A.M., Boer, R.G. den, "Transonic Wind Tunnel Investigation of Limit Cycle Oscillations on Fighter Type Wings – Update", 33rd AIAA/ASME/ASCE/AHS/ASC SDM Conference, Dallas, Texas, April 13-17, 1992.
10. Cunningham, Jr., A.M., "The Role of Shock-Induced Trailing-Edge Separation in Limit Cycle Oscillations", NASA-CP-3022, 1987.
11. Cunningham, Jr., A.M., "Practical Problems: Airplanes", Chapter 3, Unsteady Transonic Aerodynamics, edited by D.L. Nixon, AIAA Progress in Astronautics and Aeronautics Series, 1989.
12. Meijer, J.J., Zwaan, R.J., "Investigation of a Semi-empirical Method to Predict Limit Cycle Oscillations of Modern Fighter Aircraft", AGARD CP No. 483, April 1990.
13. Meijer, J.J., Cunningham, Jr., A.M., Zwaan, R.J., "A Semi-Empirical Approach to Predict Transonic Limit Cycle Oscillation Characteristics of Fighter Aircraft", 8th Aircraft/Stores Compatibility Symp., Fort Walton Beach, Florida, 23-25 October 1990.
14. Meijer, J.J., Cunningham, Jr., A.M., "Development of a Method to Predict Transonic Limit Cycle Oscillation Characteristics of Fighter Aircraft", AGARD SMP Specialist Meeting on Transonic Unsteady Aerodynamics and Aeroelasticity, San Diego, California, 9-11 October 1991.
15. Elbers, W.K., "Wind Tunnel Data Report 1/9-Scale F-16A Pressure Model Investigation of Shock-Induced Separation for Limit Cycle Oscillation Studies (AEDC PWT-16T Test TF-695)", General Dynamics, Fort Worth Division Report 16PR4694, September 1985, (Contract No. F33657-84-C-2034).
16. Cunningham, Jr., A.M., Spragle, G.S., "A Study of the Effects of Reynolds Number and Mach Number on Constant Pressure Coefficient Jump for Shock-Induced Trailing-Edge Separation", NASA-CR-4090, August 1987.
17. Triebstein, H., "Steady and Unsteady Transonic Pressure Distributions on NACA 0012", Journal of Aircraft, Vol.23, No.3, March 1986, pp. 213-219.
18. Edwards, J.W., Bennett, R.M., Whitlow, Jr., W., Seidel, D.A., "Time-marching Transonic Flutter Solutions including Angle-of-attack Effects", J. Aircraft, Vol. 20, No. 11, Nov. 1983, pp. 899-906.
19. Mabey, D.G., "Physical Phenomena Associated with Unsteady Transonic Flows", Chapter 1, Unsteady Transonic Aerodynamics, edited by D.L. Nixon, AIAA Progress in Astronautics and Aeronautics Series, 1989.
20. Dat, R. "Development of the Basic Methods Needed to Predict the Aeroelastic Behavior of Helicopters", Rech. Aerosp. 1983-1.
21. Petot, D., "Differential Equation Modeling for Dynamic Stall", Rech. Aerosp. 1989-5.
22. McAlister, K.W., Lambert, O., Petot, D., "Application of the Onera Model of Dynamic Stall", NASA TP2399 or AVSCOM TP84-A-3, 1984.
23. Leishman, J.G., Crouse, Jr., G.L., "State-space Model for Unsteady Airfoil Behavior and Dynamic Stall", AIAA-89-1319.
24. Reddy, T.S.R., Kaza, K.R.V., "A Comparitive Study of Some Dynamic Stall Models", NASA TM 88917, 1987.
25. Bland, S.R., "Transonic Unsteady Aerodynamics and Aeroelasticity 1987", NASA CP 3022, 1987.
26. Cunningham, Jr., A.M., Coe, C.F., "Predictions of F-111 TACT Aircraft Buffet Response", AGARD CP No. 483, April 1990.